Study on Nonlinear Dynamic Response of an Unbalanced Rotor Supported on Ball Bearing

G. Chen
College of Civil Aviation,
Nanjing University of Aeronautics and
Astronautics,
Nanjing, 210016, P.R.C.
e-mail: cgzyx@263.net

An unbalanced rotor dynamic model supported on ball bearings is established. In the model, three nonlinear factors of ball bearing are considered, namely, the clearance of bearing, nonlinear Hertzian contact force between balls and races, and the varying compliance vibrations because of periodical change in contact position between balls and races. The numerical integration method is used to obtain the nonlinear dynamic responses; the effects of the rotating speed and the bearing clearance on dynamic responses are analyzed; and the bifurcation plots, the phase plane plots, the frequency spectra, and the Poincaré maps are used to carry out the analyses of bifurcation and chaotic motion. Period doubling, quasiperiod loop breaking, and mechanism of intermittency are observed as the routes to chaos. [DOI: 10.1115/1.3142883]

1 Introduction

At present, in the research of rotor dynamics, the effect of bearings on rotor dynamic responses has already been taken fully into account and the rotor-bearing system dynamics has been developed [1]. In the research of rotor-bearing system dynamics, the current main research work is to carry out mechanism analyses of single and coupling faults, such as dynamic analyses of crack rotor under nonlinear oil-film force [2,3], rubbing rotor [4,5], and pedestal looseness rotor [6–9] and so on.

Nowadays, the dynamic responses of a fault rotor supported on oil sliding bearings have been studied extensively, however, the dynamic model of a fault rotor supported on ball bearings is still very immature [10–12], and the ball bearings' clearance and the varying compliance (VC) vibration are not considered.

In the research on ball bearing vibrations, although the model of ball bearings is almost perfect, it is not combined well with the rotor vibration. Fukata et al. [13] and Mevel and Guyader [14] only considered the parameter excitation (VC vibration), which comes from varying stiffnesses, but not the effect of rotor unbalance; the unbalance force and bearing clearance were considered by Kim and Noah [15,16], but not VC vibration; the combined effect of unbalance, bearing clearance, nonlinear Hertzian contact force, and VC vibration were studied by Tiwari and Gupta [17]; but the unbalance force was considered as a constant force throughout the rotating speed range. The works of Bai and Xu [18] considers the effects of clearance, race waviness, and unbalance on the cage speed and the high-speed effects of ball centrifugal forces and gyroscopic moment, but the rotor is only considered as a participating mass so that the first-order bending vibration of rotor cannot be simulated. Therefore, these models all have some disadvantages.

In this paper, a new nonlinear dynamic model of an unbalance rotor supported on ball bearings is established, in which not only the rotor unbalance, bearing clearance, nonlinear Hertzian contact force, and VC vibration are considered together, but also the unbalance force that varies with rotating speed. In addition, in the new rotor-bearing model, the mass of rotor includes three parts, namely, rotor mass at the rotor disk, left bearing, and right bearing, and the first-order bending vibration can then be simulated. Rotor responses are obtained by numerical integration, and the

effects of rotating speed and bearing clearance on system responses are studied. The bifurcation plots, the phase plane plots, the frequency spectra, and the Poincaré maps are used to analyze the characteristics of bifurcation and chaos of system responses. Three routes to chaos are observed.

2 Dynamic Model of a Rotor Supported on Ball Bearing

2.1 Dynamic Equations. In this paper, a new dynamic model of an unbalance rotor supported on ball bearings is set up, and Fig. 1 shows the schematic of this model. In this model, the two ends of this rotor are supported on similar ball bearings. The new rotor-bearing model, which is established in this paper, combines the rotor model, which makes reference to the literature [1], and the ball bearing model, which makes reference to the literature [13]. The rotor model in this paper is assumed symmetrical to the central plane and the gyroscopic forces are neglected.

Figure 1 Notations and Variables: O_1, O_2, O_3—bearing geometric center, rotor geometric center, and rotor center of mass; m_{rp}—equivalent mass of rotor at the disk; m_{rL}, m_{rR}—rotor equivalent mass at the left and the right bearings, they include the inner ring mass and the rotor mass which is installed into bearing; c_{rp}, c_{rb}—damping coefficient of rotor at the disk and bearing; k—the stiffness of the elastic shaft; e—rotor eccentricity distance; F_{xL}, F_{yL}—supporting force components in the X and Y directions of left bearing; F_{xR}, F_{yR}—supporting force components in the X and Y directions of right bearing.

The system differential equations of motion can be obtained as follows:

$$m_{rp}\ddot{x}_{rp} + c_{rp}\dot{x}_{rp} + k(x_{rp} - x_{rR}) + k(x_{rp} - x_{rL}) = m_{rp}e\omega^2 \cos(\omega t)$$

$$m_{rp}\ddot{y}_{rp} + c_{rp}\dot{y}_{rp} + k(y_{rp} - y_{rR}) + k(y_{rp} - y_{rL})$$
$$= m_{rp}e\omega^2 \sin(\omega t) - m_{rp}g$$

$$m_{rR}\ddot{x}_{rR} + c_{rb}\dot{x}_{rR} + k(x_{rR} - x_{rp}) = F_{xR}$$

$$m_{rR}\ddot{y}_{rR} + c_{rb}\dot{y}_{rR} + k(y_{rR} - y_{rp}) = F_{yR} - m_{rR}g \qquad (1)$$

$$m_{rL}\ddot{x}_{rL} + c_{rb}\dot{x}_{rL} + k(x_{rL} - x_{rp}) = F_{xL}$$

$$m_{rL}\ddot{y}_{rL} + c_{rb}\dot{y}_{rL} + k(y_{rL} - y_{rp}) = F_{yL} - m_{rL}g$$

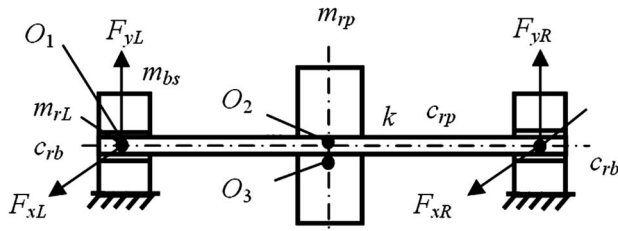where ω is the rotor angular speed.

Fig. 1 Unbalance rotor-ball bearing dynamic model

2.2 Ball Bearing Model.

Ball bearing consists of inner race, outer race, and rolling balls and cages. The outer race acts on the inner race by rolling balls, and their interaction force is a restoring force, which is generated by the contact deformation between balls and races. In the rotor-ball bearing system, usually, the outer race of the ball bearing is fixed to the bearing housing and the inner race is rigidly fixed to the rotating shaft. When ball bearing works, with the contact position between balls and races periodically varying, the total stiffness and compliance of bearing vary periodically, and the varying compliance of bearing is a parametric excitation of the rotor-balling bearing coupling system; hence, the so-called varying compliance (VC) vibration is generated. VC vibration is an inherent vibration, and it always exists even if the bearing is newly installed and is fault-free.

Figure 2 is a schematic of a ball bearing model, which makes reference to the literature [13]. The excitations of ball bearing come from two aspects: one is the rotor imbalance, and the other is the continuous periodic change in the total stiffness of the bearing, which is a parametric excitation.

In the ball bearing model, it is supposed that the balls are equispaced between the surfaces of the inner and the outer races, and the contact angles are not considered. V_{in} is the tangent velocity of the contact point between the ball and the inner race; ω_{inner} is the rotating angular velocity of the bearing inner race; R is the radius of the outer race; and r is the radius of the inner race. Therefore,

$$V_{in} = \omega_{inner} \times r \qquad (2)$$

and, the tangent velocity of the cage is

$$V_{cage} = V_{in}/2 = (\omega_{inner} \times r)/2 \qquad (3)$$
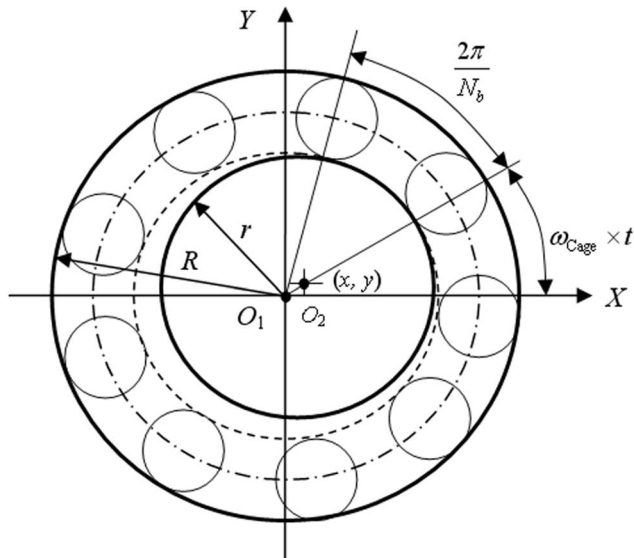
Therefore, the angular velocity of the cage is given by

Fig. 2 Schematic of the ball bearing

$$\omega_{cage} = \frac{V_{cage}}{(R+r)/2} = \frac{(\omega_{inner} \times r)/2}{(R+r)/2} = \frac{\omega_{inner} \times r}{(R+r)} \qquad (4)$$

Because the inner race is fixed to the shaft, $\omega_{inner} = \omega_{rotor}$. If N_b is the number of balls, and then VC frequency can be given by

$$\omega_{VC} = \omega_{cage} \times N_b = \omega_{rotor} \times \left(\frac{r}{R+r} \times N_b\right) = \omega_{rotor} \times BN \quad (5)$$

where

$$BN = \frac{r}{R+r} \times N_b \qquad (6)$$

Obviously, the variable BN depends on the dimensions of the bearing.

Assume the angle location of the jth ball is θ_j, which is given by $\theta_j = \omega_{cage} \times t + 2\pi/N_b(j-1)$, $j = 1, 2, \ldots, N_b$. Also, assume x and y are the vibration displacements of the center of the inner race in the X and Y directions, respectively, and $2r_0$ is the bearing clearance. Therefore, the normal contact deformation between the jth ball and races is given by

$$\delta_j = x \cos \theta_j + y \sin \theta_j - r_0 \qquad (7)$$

According to the nonlinear Hertzian contact theory, the contact force f_j between ball and race due to the rolling contact can be obtained. At the same time, because the ball at angular location θ_j can only result in a normal positive restoring force f_j, f_j must be greater than zero. Therefore, only $\delta_j > 0$ for the contact force can appear. By introducing the function $H(x)$ defined as

$$H(x) = \begin{cases} 1, & x > 0 \\ 0, & x \le 0 \end{cases} \qquad (8)$$

f_j can be obtained as follows:

$$f_j = C_b[\delta_j]^{3/2} = C_b(x \cos \theta_j + y \sin \theta_j - r_0)^{3/2}H(x \cos \theta_j + y \sin \theta_j - r_0) \qquad (9)$$

where C_b is the Hertzian contact stiffness and depends on the contact material and shape. The components of f_j in the X and Y directions are as follows:

$$f_{jx} = C_b(x \cos \theta_j + y \sin \theta_j - r_0)^{3/2}H(x \cos \theta_j + y \sin \theta_j - r_0)\cos \theta_j \qquad (10)$$

$$f_{jy} = C_b(x \cos \theta_j + y \sin \theta_j - r_0)^{3/2}H(x \cos \theta_j + y \sin \theta_j - r_0)\sin \theta_j$$

Therefore the bearing forces generated by the ball bearing are given by

$$F_x = \sum_{j=1}^{N_b} f_{jx} = \sum_{j=1}^{N_b} C_b(x \cos \theta_j + y \sin \theta_j - r_0)^{3/2}$$
$$\times H(x \cos \theta_j + y \sin \theta_j - r_0)\cos \theta_j$$

$$\qquad (11)$$

$$F_y = \sum_{j=1}^{N_b} f_{jy} = \sum_{j=1}^{N_b} C_b(x \cos \theta_j + y \sin \theta_j - r_0)^{3/2}$$
$$\times H(x \cos \theta_j + y \sin \theta_j - r_0)\sin \theta_j$$

Therefore, the bearing forces in Fig. 1 can be obtained by the following:

(1) When $x = x_{rR}$, $y = y_{rR}$, then $F_{xR} = F_x$, $F_{yR} = F_y$.
(2) When $x = x_{rL}$, $y = y_{rL}$, then $F_{xL} = F_x$, $F_{yL} = F_y$.

2.3 Original Dynamic Parameters.

In this paper, making reference to literature [1], the original parameters of the rotor system are chosen as follows: $m_{rR} = m_{rL} = 4.0$ kg, $m_{rp} = 32.1$ kg, $c_{rb} = 1050$ N s/m, $c_{rp} = 2100$ N s/m, $k = 2.5 \times 10^7$ N/m, and $e = 0.01$ mm.

The JIS6306 ball bearing in Ref. [13] is chosen as the ball

Table 1 The main parameters of the JIS6306 ball bearing

Radius of the outer race, R (mm)	Radius of the inner race, r (mm)	No. of balls, N_b	Contact stiffness, C_b (N/m$^{3/2}$)	Bearing clearance, $2r_0$ (μm)	BN
63.9	40.1	8	13.34×10^9	40	3.08

bearing in this paper, and its parameters are listed in Table 1.

In order to study in depth the dynamic behavior of an unbalance rotor supported on ball bearings, the system dynamic responses need to be obtained. There are many methods to obtain the periodic solution of the nonlinear system, but numerical methods are the most efficient approach to study the quasiperiodic and chaos phenomena. Because of the very strong nonlinearity of the rotor-ball bearing system, the Runge–Kutta–Fehlberg method [19] is used to solve differential equations and obtain the responses of the rotor-ball bearing system.

3 Dynamic Behavior Analysis of an Unbalanced Rotor Supported on Ball Bearing

3.1 Model Verifying. In the reference, a dynamic model of an unbalanced rotor supported on ball bearings, which are subject to a constant vertical radial load, was established by Mevel and Guyader [14], and the sixth order Runge–Kutta method was used to obtain the responses of the rotor.

In order to verify the new rotor-bearing model, in this paper, the simulation results of the new model should be compared with the results of Mevel and Guyader [14] based on the same computation conditions. The rotor parameters are determined as: $m_{rR} = m_{rL}$ = 2.0 kg, m_{rp} = 8 kg, c_{rb} = 200 N s/m, c_{rp} = 2940 N s/m, k = 2.5 $\times 10^8$ N/m, e = 0.01 mm. The identical ball bearing as reference [14] is used, and its parameters are listed in Table 1.

In the rotor model of Mevel and Guyader [14], the rotor is considered as only one participating vibration mass so that the rotor bending vibration cannot be simulated; in order to approximate the rotor model of Mevel and Guyader [14], in the computation conditions, the rotor stiffness k is so great that the rotor vibrates as a whole and the bending vibration of the rotor is not generated.

Figures 3(a) and 4(a) are, respectively, the vibration displacements in the X and Y directions at the rotor disk at a rotating speed of 300 rpm; Figs. 3(b) and 4(b) are, respectively, the vibration displacements in the X and Y directions at the rotor disk at a rotating speed of 300 rpm in Ref. [14] by Mevel and Guyader. Obviously, their results are almost identical; therefore, the correctness of the new rotor-bearing model is fully verified.

Because the excitations of the unbalanced rotor supported on ball bearing come from two aspects—one is rotating frequency excitation from unbalance, and the other is the VC frequency excitation from the periodic variety of bearing stiffness—when the rotating speed is very low, unbalance force is very weak, and the VC vibration can be observed clearly because of the periodic variety of bearing stiffness. Hereinto, the frequency of VC vibration
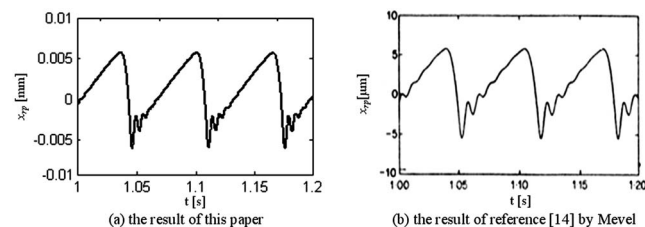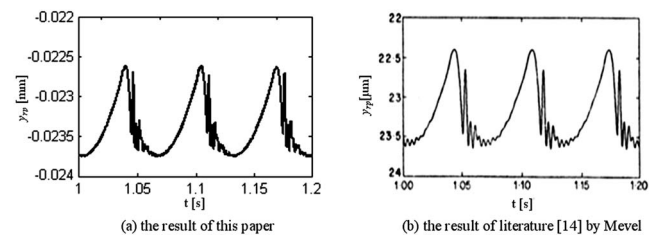
is BN times the rotating frequency. In this paper, the value of BN is 3.08, as shown in Table 1. From the frequency spectra of signals shown in Figs. 5(a) and 5(b), it can be seen that the rotor vibration represents the VC frequency (the ball passage frequency) and its harmonics.

According to the literature [13], for the JIS6306 ball bearings, the natural frequencies in the X and Y directions are f_x = 101.5 Hz and f_y = 259 Hz, respectively. The two critical speeds of the bearing assembly are defined by a ball pass frequency f_b equal to one of the resonant frequency, and f_b = 0.05139 n_r, hereinto the n_r is the rotating speed. Thus, the two critical speeds in the X and Y directions are n_x = 1976 rpm and n_y = 5040 rpm, respectively. The study of Fukata et al. [13] shows that when the rotating speed is far from the two critical rotating speeds in the X and Y directions, the motion is periodic and represents the ball passage frequency and its multiple harmonic components. Apparently, the result of this paper accords with the conclusion, therefore, the correctness of the new rotor-bearing model is further verified.
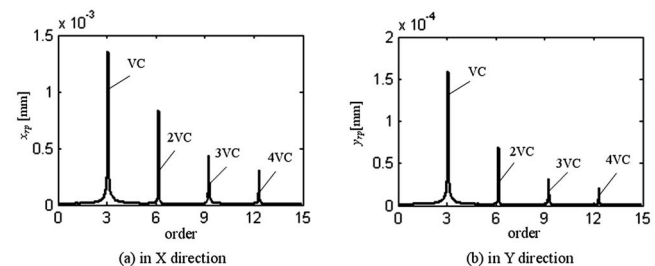
3.2 The Effect of Rotating Speed on System Responses. With the rotating speed increasing, the excitation of the unbalance force is strengthened, and in the system responses, the component of the rotating frequency gradually increases. Figures 6 and 7 are, respectively, the frequency spectrum and Poincaré map of the rotor disk displacement in the X directions at a rotating speed of 3000 rpm. When the rotating speed increases to 4000 rpm, these results are shown in Figs. 8 and 9; when the rotating speed increases to 5000 rpm, they are shown in Figs. 10 and 11; when the rotating speed increases to 6000 rpm, they are shown in Figs. 12 and 13; when the rotating speed increases to 7000 rpm, they are shown in Figs. 14 and 15; and finally when the rotating speed increases to 8000 rpm, the results are shown in Fig. 16 and 17.

Here, the displacement and the velocity of system response are

(a) the result of this paper

(b) the result of literature [14] by Mevel

Fig. 4 The rotor response in the Y direction at rotor disk (n_r = 300 rpm)

(a) the result of this paper

(b) the result of reference [14] by Mevel

Fig. 3 The rotor response in the X direction at rotor disk (n_r = 300 rpm)

(a) in X direction

(b) in Y direction

Fig. 5 The rotor response spectra at rotor disk (n_r = 300 rpm)
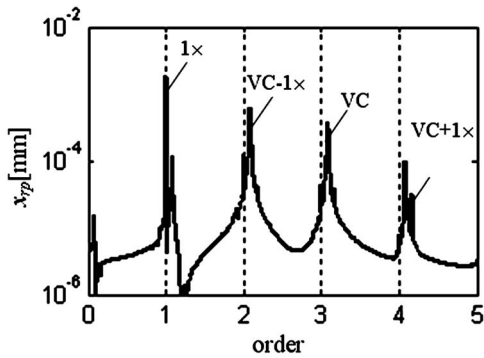
Fig. 6 Spectrum (n_r=3000 rpm)

Fig. 9 Poincaré map (n_r=4000 rpm)

sampled at every rotating period, the displacement sampling points are acted as the *x*-coordinate, the velocity sampling points are acted as the *y*-coordinate, and the Poincaré map is obtained. If the system response has *n* periodic solutions, there are *n* isolated points in its Poincaré map; if the system response is quasiperiodic, there are some close curves in its Poincaré map; if the system response is chaos, there are a piece or many pieces of dispersed points in its Poincaré map.

In this paper, the ratio *BN* of VC frequency to rotating frequency is an irrational number, because *BN* is given by $BN=N_b \times r/(R+r)=401/130\approx3.08$. From the frequency spectrum shown in Figs. 6, 8, 10, 12, 14, and 16, it can be seen that there are rotating frequency components and its harmonics, VC frequency component and its harmonics, and the sum and difference of the combination frequency components in these frequency spectra. The four varying phases of the system state can be found as follows. (1) When the rotating speed is very low, vibration response mainly includes the rotating frequency component and its harmonics and the VC frequency component and its harmonics; therefore,

the system motion is quasiperiodic, and there is a close curve in its Poincaré map, which is shown in Fig. 7. (2) With the speed increasing, the rotating frequency component gradually increases in the system response. From Figs. 8, 10, and 12, we can find out that the different combinations of frequency components give birth to more frequency components, but the system motion is still quasiperiodic because their Poincaré maps still show the close curves in Figs. 9, 11, and 13. (3) With the speed continuously increasing, when the speed is close to the first-order critical speed, as shown in Fig. 14, the rotating frequency components increase quickly, the VC frequency components and the combination frequency components decrease relatively, and the system enters the period 1 motion, where there is only one isolated point in its Poincaré map, as shown in Fig. 15. (4) When speed exceeds the first critical speed, the more combination frequency components and subharmonics come forth, and the continuous frequency spectra appear in Fig. 16; at the same time, pieces of dispersed points like a cloudlet come forth in the Poincaré maps, as shown in Fig. 17. Obviously, the system shifts into a chaotic state.
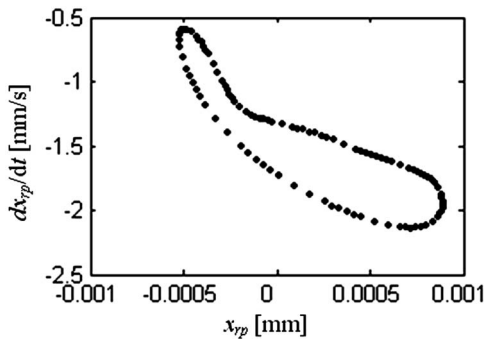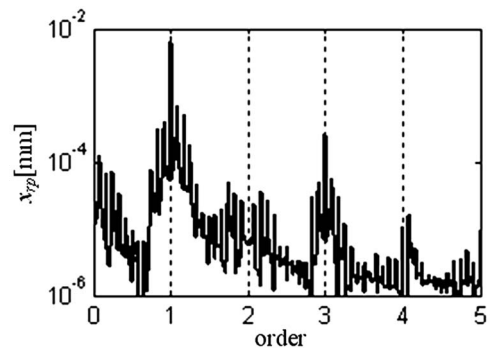

Fig. 7 Poincaré map (n_r=3000 rpm)
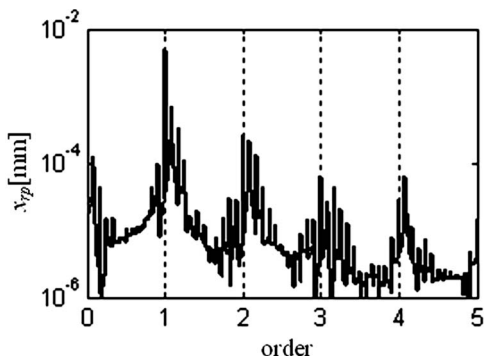

Fig. 10 Spectrum (n_r=5000 rpm)

Fig. 8 Spectrum (n_r=4000 rpm)
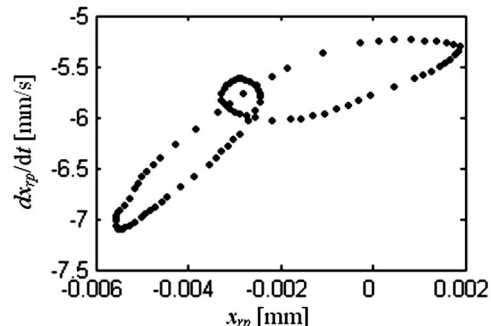

Fig. 11 Poincaré map (n_r=5000 rpm)
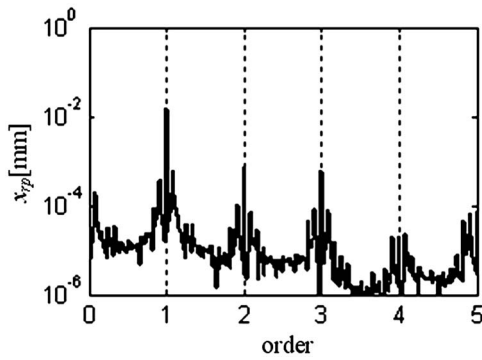
Fig. 12   Spectrum (n_r=6000 rpm)

Fig. 15   Poincaré map (n_r=7000 rpm)

3.3   The Effect of Bearing Clearance on the Bifurcation of the Rotor Motion. Due to the installation and employing of ball bearings, some clearances are inherent to the process. This clearance is a very strong nonlinear factor in the system dynamics. In addition, there are other nonlinear factors in ball bearing such as the nonlinear Hertzian contact force and the nonlinear total stiffness. Under certain conditions, the nonlinear system will give birth to bifurcation. In order to study the effect of the bearing clearance on the bifurcation behavior of the system, in this paper the bifurcation plots under different bearing clearances are obtained by numerical integration and the routes to chaos are analyzed.

Figure 18 shows the bifurcation plots with bearing clearance of 0 μm. From the plots it can be seen that when the rotating speed is lower than 5000 rpm, the system motion is quasiperiodic because of the concurrence of the rotating frequency component and VC frequency component. When the rotating speed is higher than 5000 rpm, because the VC vibration of the system is relatively weak, the system motion is periodic and the system does not
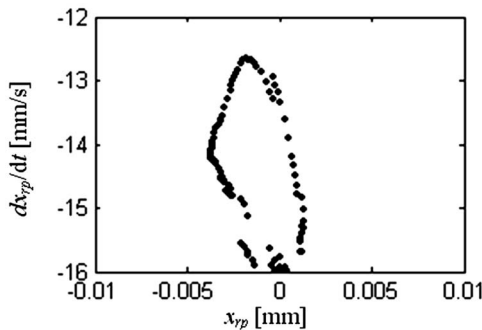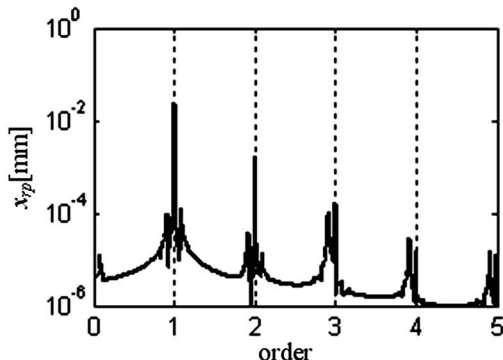
appear to engage in chaos regime.

Figure 19 shows the bifurcation plots with bearing clearance of 10 μm. According to the Fig. 19, the system motion can be divided into the following six segments:

(1) *Segment A (2000–5000 rpm).* Because of the concurrence of the rotating frequency component and VC frequency component in the system, the system motion is quasiperiodic.

(2) *Segment B (5000–12,000 rpm).* When the rotating speed is near the first-order critical speed, the unbalance response becomes very great, and the VC vibration of the system is relatively weak. Thus, the system enters the period 1 motion.

(3) *Segment C (12,000–13,500 rpm).* As the rotating speed gradually increases, period-doubling appears (Fig. 20(*a*)).When the fractional harmonic components combine each other with VC vibration in the way of sum and difference, the quasiperiod loop starts to break (Fig. 20(*b*)) and chaos appears (Fig. 20(*c*)). Finally, through inverse bifur-
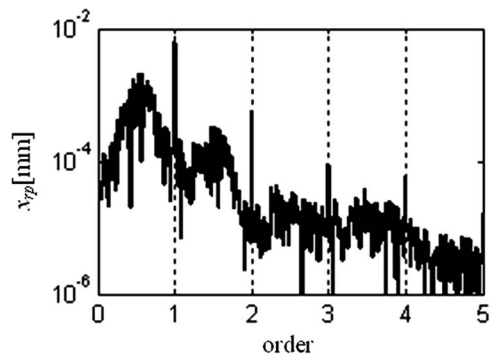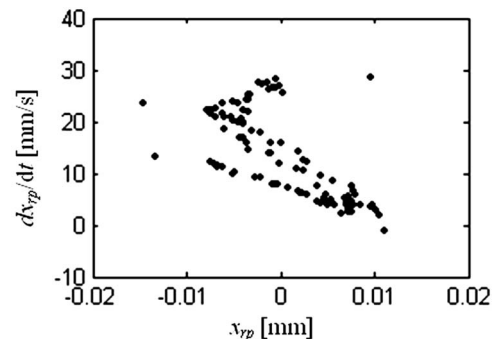

Fig. 13   Poincaré map (n_r=6000 rpm)

Fig. 14   Spectrum (n_r=7000 rpm)

Fig. 16   Spectrum (n_r=8000 rpm)

Fig. 17   Poincaré map (n_r=8000 rpm)
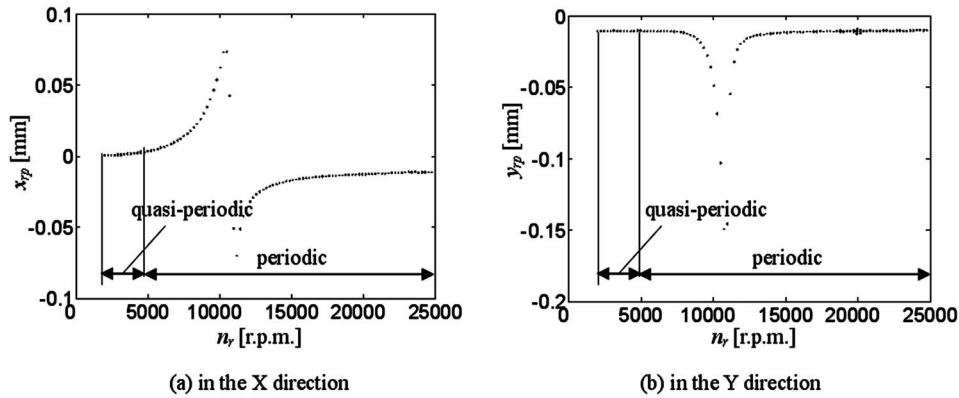
(a) in the X direction   (b) in the Y direction

Fig. 18 The bifurcation plots (clearance is 0 μm)

cation, system gets out of the chaotic regime and returns to period 1 motion. Apparently this route to chaos is from period 1 to period *n* through frequency-dividing, to quasi-periodic through frequency combination, and to chaos through quasiperiod loop breaking.

(4) *Segment D (13,500–19,000 rpm)*. This is a typical route of period-doubling bifurcation. As the rotating speed increases, period-doubling appears (according to Fig. 21(*a*)). When the rotating speed continually increases, chaos appears (according to Fig. 21(*b*)). Finally through inverse bifurcation the system gets out of the chaotic regime (according to Fig. 21(*c*)).

(5) *Segment E (19,000–20,000 rpm)*. When the rotating speed is around 20,000 rpm, in the system response, the period and chaos appear by turns; therefore, this is a typical chaos phenomenon of intermittency. From the time waveform, the phase plane plot, and the Poincaré map shown in Fig. 22,

two kinds of quasiperiodic motions appear by turns. Obviously, this is a route of intermittency to chaos.

(6) *Segment F (20,000–25,000 rpm)*. As shown in Figs. 23 and 24, at the rotating speed of 20,053 rpm, the system motion is periodic; at the rotating speed of 21,963 rpm, 1/8 fractional harmonic components appear and the system motion is periodic 8; when the rotating speed reaches 23,873 rpm, because of the combination of the many irreducible frequency components, the system motion state is quasiperiodic. Therefore, in this segment, chaos does not appear.

Figures 25–27 are the system bifurcation plots with bearing clearance of 20 μm, 40 μm and 80 μm, respectively. From the bifurcation plots, it can be seen that with the bearing clearance increasing, the segments of the rotating speeds of the quasiperiodic and chaos motions are more and wider, and intermittency and period-doubling bifurcation can be observed as the routes to
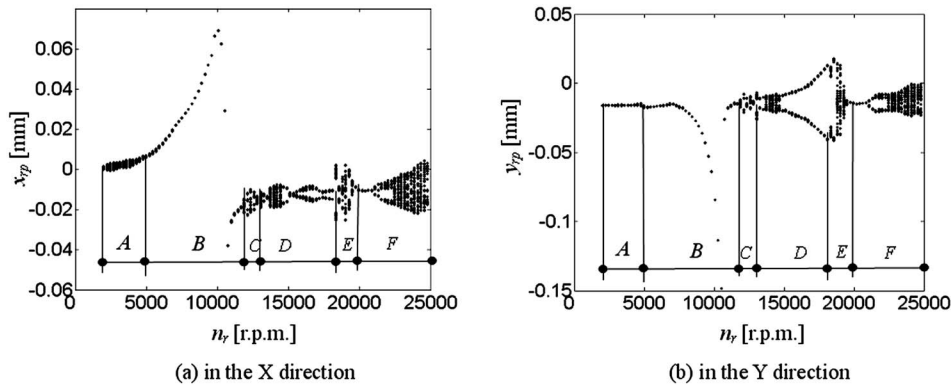

(a) in the X direction   (b) in the Y direction

Fig. 19 The bifurcation plots (clearance is 10 μm)

(a) 12605 r.p.m.   (b) 12700 r.p.m.   (c) 12796 r.p.m.

Fig. 20 Poincaré maps of x_{rp} in segment C

(a) 13369 r.p.m.　(b) 14133 r.p.m.　(c) 14706 r.p.m.
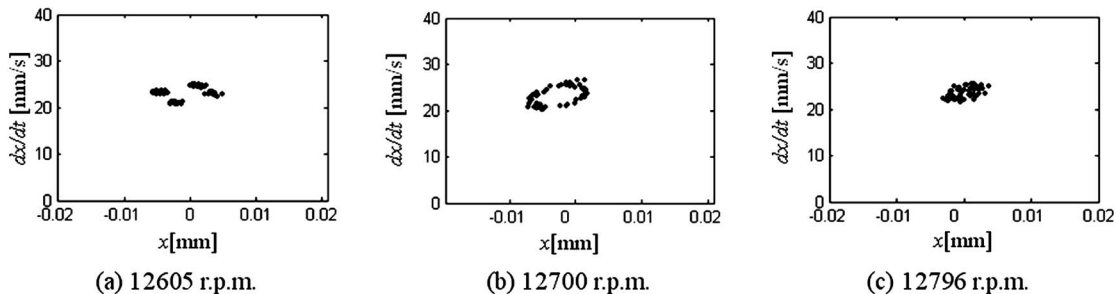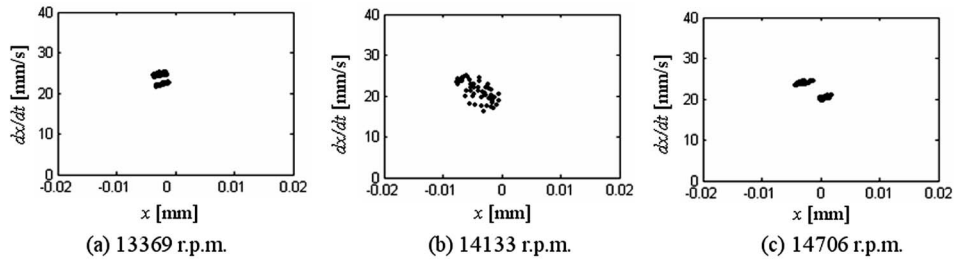
Fig. 21　Poincaré maps of x_{rp} in segment D
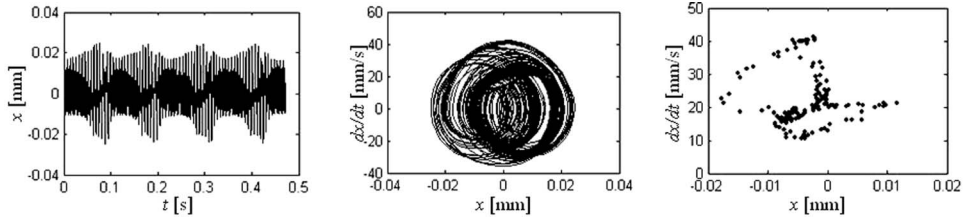
Fig. 22　Time waveform, phase plane plot, and Poincaré map of x_{rp} in segment E (n_r =19,099 rpm)
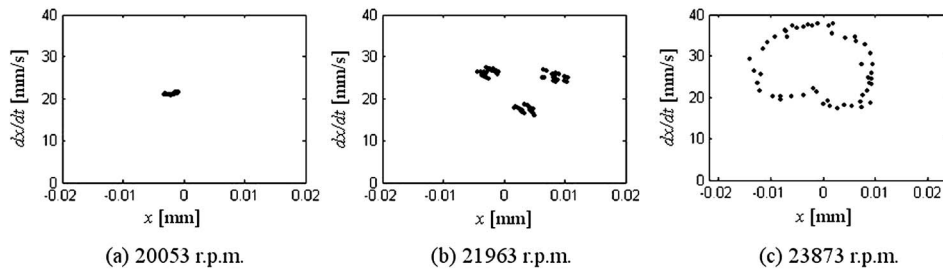

(a) 20053 r.p.m.　(b) 21963 r.p.m.　(c) 23873 r.p.m.

Fig. 23　Poincaré maps of x_{rp} in segment F

(a) 20053 r.p.m.　(b) 21963 r.p.m.　(c) 23873 r.p.m.
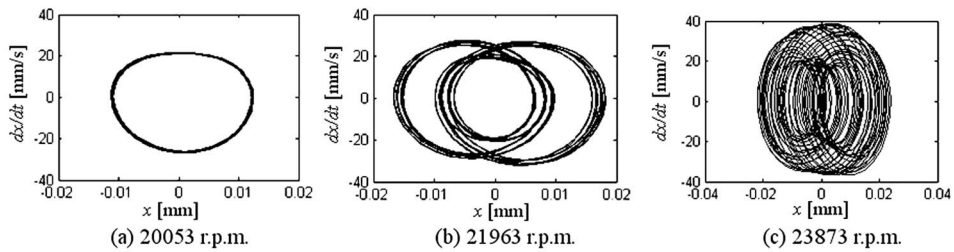
Fig. 24　Phase plane plots of x_{rp} in segment F
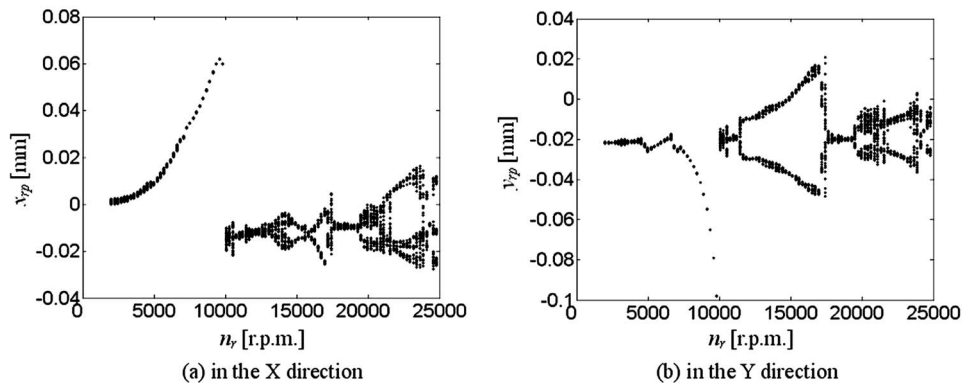

(a) in the X direction　(b) in the Y direction
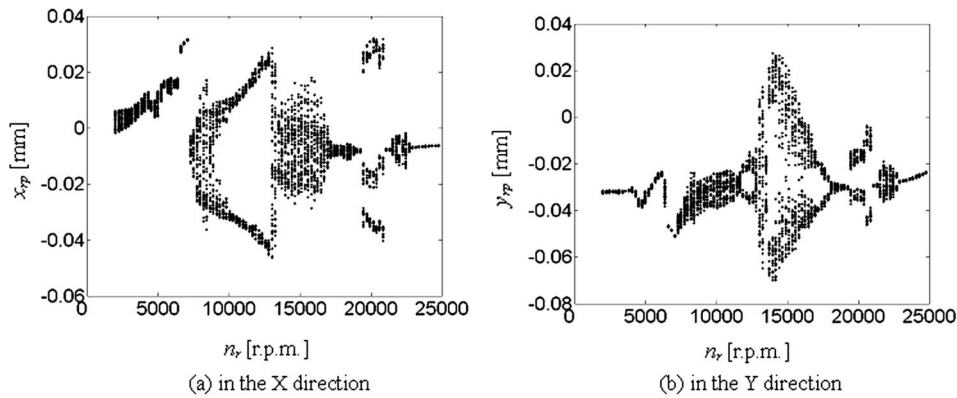
Fig. 25　Bifurcation plots (clearance is 20 μm)

Fig. 26 Bifurcation plots (clearance is 40 μm)

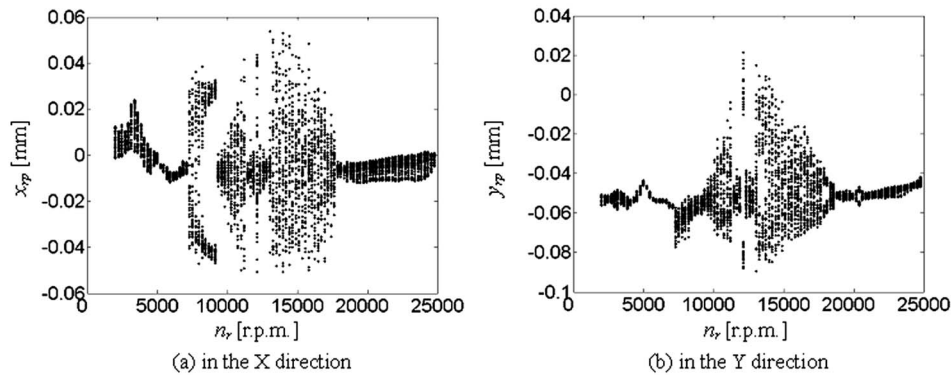**Fig. 27 Bifurcation plots (clearance is 80 μm)**

chaos. As the bearing clearance continuously increases, the duration of the chaos is longer. As can be seen, the bearing clearance has an important effect on the stability of the system.

4 Conclusions

The dynamic model of an unbalance rotor supported on the ball bearings is established. In the model, the bearing clearance, the nonlinear Hertzian contact force, and the VC vibration because of the periodic variety of the total stiffness are considered. The effect of the dynamic varying unbalance force with the rotating speed on ball bearing is considered, and a rotor model with three masses is established. The Runge–Kutta–Fehlberg method is used to calculate the system responses.

The new model is verified by comparing with the computing results of Mevel and Guyader [14] based on the same rotor and bearing parameters, and the results fully show the correctness of the new model. The effect of the rotating speed on the rotor-bearing system responses is analyzed, and many combination frequency components of rotating frequency and VC frequency are found with rotating speed increasing gradually.

The phenomena of the system bifurcation and the effect of the bearing clearance on the system motion are studied. Period-doubling bifurcation, quasiperiod loop breaking, and mechanism of intermittency are observed as the routes to chaos. By comparing the bifurcation plots under the various bearing clearances, it is found out that the larger the bearing clearance, the longer the duration of chaos and the worse the stability of the system. Therefore, in the process of design and operation of the ball bearing, it is necessary to effectively control the ball bearing clearance.

References

[1] Wen, B. C., Wu, X. H., and Han, Q. K., 2004, *The Nonlinear Dynamics Theory and Experiments of Rotating Mechanism With Faults*, Science Press, Beijing, China, pp. 1–10, in Chinese.
[2] Mayes, I. W., 1984, "Analysis of the Response of a Multi-Rotor-Bearing System Containing a Transverse Crack in a Rotor," Trans. ASME, J. Vib., Acoust., Stress, Reliab. Des., **106**, pp. 139–145.
[3] Meng, G., 1992, "The Nonlinear Influences of Whirl Speed on the Stability and Response of a Cracked Rotor," Journal of Machine Vibration, **4**, pp. 216–230.
[4] Muszynska, A., 1984, "Partial Lateral Rotor to Stator Rubs," *Proceedings of the Third International Conference on Vibration in Rotating Machinery*, Yorkshire, UK, Paper No. C281/84, pp. 327–335.
[5] Muszynska, A., 1988, "Stability of Whirl and Whip in Rotor Bearing System," J. Sound Vib., **127**(1), pp. 49–64.
[6] Goldman, P., and Muszynska, A., 1991, "Analytical and Experimental Simulation of Loose Pedestal Dynamic Effects on a Rotating Machine Vibration Response," 13th Biennial Conference on Mechanical Vibration and Noise, Miami, FL, pp. 29–39.
[7] Ji, Z., and Zu, J. W., 1998, "Method of Multiple Scales for Vibration Analysis of Rotor-Shaft Systems With Non-Linear Bearing Pedestal Model," J. Sound Vib., **218**(2), pp. 293–305.
[8] Lee, A. C., Kang, Y., and Liu, S. L., 1991, "A Modified Transfer Matrix for the Linear Rotor-Bearing System," ASME J. Appl. Mech., **58**, pp. 776–783.
[9] Lee, A. C., Kang, Y., and Liu, S. L., 1993, "Steady Analysis of a Rotor Mounted on Nonlinear Bearings by the Transfer Matrix Method," Int. J. Mech. Sci., **35**, pp. 479–490.
[10] Choi, B. L., and Part, J. M., 2001, "An Improved Rotor Model With Equivalent Dynamic Effects of the Support Structure," J. Sound Vib., **244**(4), pp.

569–581.

[11] Chen, E. L., He, T., and Zheng, M., 2004, "Study on Complicated Motion of Roll Element Bearing-Rotor System With Pedestal Looseness," J. Dyn. Control Syst., **2**(4), pp. 49–54.

[12] Liu, X. D., He, T., and Li, Q. H., 2005, "Dynamic Model of Rotor System With Support Loosening and its Diagnosis Method," Journal of Aerospace Power, **20**(1), pp. 56–59.

[13] Fukata, S., Gad, E. H., and Kondou, T., 1985, "On the Radial Vibration of Ball Bearings (Computer Simulation)," Bull. JSME, **28**, pp. 899–904.

[14] Mevel, B., and Guyader, J. L., 1993, "Routes to Chaos in Ball Bearings," J. Sound Vib., **162**(3), pp. 471–487.

[15] Kim, Y. B., and Noah, S. T., 1990, "Bifurcation Analysis for a Modified Jeffcott Rotor With Bearing Clearances," Nonlinear Dyn., **1**, pp. 221–241.

[16] Kim, Y. B., and Noah, S. T., 1996, "Quasi-Periodic Response and Stability Analysis for a Non-Linear Jeffcott Rotor," J. Sound Vib., **190**(2), pp. 239–253.

[17] Tiwari, M., and Gupta, K., 2000, "Dynamic Response of an Unbalanced Rotor Supported on Ball Bearings," J. Sound Vib., **238**(5), pp. 757–779.

[18] Bai, C. Q., and Xu, Q. Y., 2006, "Dynamic Model of Ball Bearings With Internal Clearance and Waviness," J. Sound Vib., **294**, pp. 23–48.

[19] Mathews, J. H., and Fink, K. D., 2005, *Numerical Methods Using MATLAB*, 4th ed., Electronics Industry Press, Beijing, China.